

<https://doi.org/10.1038/s42005-025-02386-6>

Relationship between hydrogen diffusion and negative-SET occurred in resistive random access memory with inert electrode

Check for updates

Yiwei Duan¹, Xudong Feng¹, Yuqi Liu¹, Haifeng Yang¹, Fei Liu¹ ✉, Yu Qian¹ ✉ & Yintang Yang^{2,3} ✉

The negative-SET occurred in resistive random access memory (RRAM) leads to irreversible hard breakdown, and it is urgent to investigate the reasons for its occurrence. In this paper, we use Pt and Ru inert electrodes with different hydrogen diffusion coefficients to construct SiNx-based RRAM, and the relationship between hydrogen ion movement and the occurrence of negative-SET is studied. By analyzing the test results of current sweep mode and fitting results of current conduction mechanisms, we proposed that the diffusion of hydrogen ions from the switching layer to the electrode is the key cause of the occurrence of the negative-SET process. This study suggests that the role of hydrogen ions in the switching process should be incorporated into the RRAM model, and we should pay more attention to the influence of hydrogen diffusion on the characteristics of RRAM, especially on reliability.

In the information age, there is an urgent need for new storage hardware to achieve efficient storage and processing of the increasing volume of data^{1–3}. Valence change memory (VCM), as a mainstream type of resistive random access memory (RRAM), has received extensive attention. It has advantages of low power consumption, good scaling ability and excellent data retention characteristics, making it a core candidate for the next generation of storage technology^{4–7}. According to the resistive switching (RS) theory, a positive bias is applied to the operation electrode, anions (such as oxygen ions and nitrogen ions) move and conductive filaments (CFs) formed, and VCM switches from high resistance state (HRS) to low resistance state (LRS), which is called a positive-SET. Once the negative bias is applied to the operation electrode, the CFs broken and VCM switches from LRS to HRS, which is called negative-RESET. VCM achieve repeatable cycles through positive-SET and negative-RESET, which is a prerequisite for the normal operation of VCM⁸. Noted that negative-SET behavior has recently been observed in various VCM^{9–11}. The negative-SET of VCM means that the SET occurs again under negative voltage (instead of the RESET process), making significant changes in current level, leading to irreversible hard breakdown, i.e., programming failure, which is unacceptable^{12,13}.

At present, the research on the occurrence mechanism of negative-SET mainly focuses on VCM with reactive electrodes. It is proposed that the adsorption of anions by reactive electrodes leads to an increase in the

number of anion vacancies in the RS layer, making overgrowth of anion vacancies CFs (that is, uncontrolled changes in the size and morphology of CFs), which is the reason for the occurrence of negative-SET in VCM^{11,12,14}. However, whether through experiments or simulations, it is difficult to directly observe CFs overgrowth process, leading to the discussion on the applicability and rationality of the above theory. And due to the inert electrode does not react with the anions, thus the VCM using inert electrodes should be able to avoid the negative-SET process caused by the overgrowth of CFs according to the above theory, however, the negative-SET process is still observed by Wang et al. in Pt/HfO_x/Pt VCM with inert top and bottom electrodes¹⁵, indicating that above theory does indeed need to be further refined. We investigated the papers on the causes of negative-SET in RRAM devices, and summarized the device stacked structure, SET/RESET voltage, forming voltage and the causes of negative-SET occurred in the published papers, as shown in Table 1.

Hydrogen is a highly mobile and reactive species, which is difficult to completely remove from vacuum systems and is highly soluble in many targets used to deposition process, inevitably becoming one of the most important impurities in VCM, and its impact on the RS process cannot be ignored^{16–18}. Cox et al. reported that in Ti/SiO_x/Mo VCM, uncontrolled diffusion of hydrogen ions through the Mo electrode can lead to abnormal current fluctuations¹⁶. Wang et al. reported that introducing hydrogen ions into W/Gd₂O₃/Pt VCM can passivate interface defects and significantly

¹School of Physics and Opto-electronic Technology, Baoji University of Arts and Sciences, Baoji, China. ²Faculty of Integrated Circuit, Xidian University, Xi'an, China. ³Shaanxi Key Laboratory of Integrated Circuits and System Integration, Xi'an, China. ✉e-mail: bwllf@163.com; qianyu0272@163.com; ytyang@xidian.edu.cn

Table 1 | Performance comparison of different structural RRAM devices exhibiting negative-SET phenomenon

Stack	Forming voltage(V)	Set/Reset voltage(V)	Cycle number before negative-SET occurred	The mechanism of negative-SET occurred	References
Ni/Ti/ Al ₂ O ₃ /p-Si	4.7	3.0/-2.5	32 cycles	Accumulation of oxygen vacancies	11
Ti/TiO ₂ /Pt	1.5	0.8/-0.4	after a few switching cycles	Accumulation of oxygen vacancies	12
Pt/HfO _x /Pt	5.1	0.7/-0.6	181 cycles	Accumulation of oxygen vacancies	15
ITO/MER/Al		1.7/-2.1		Accumulation of Al ion	9
Pt/SiN _x /Ru		0.85/-0.8	after some switching cycles	Hydrogen ion diffusion	This Work

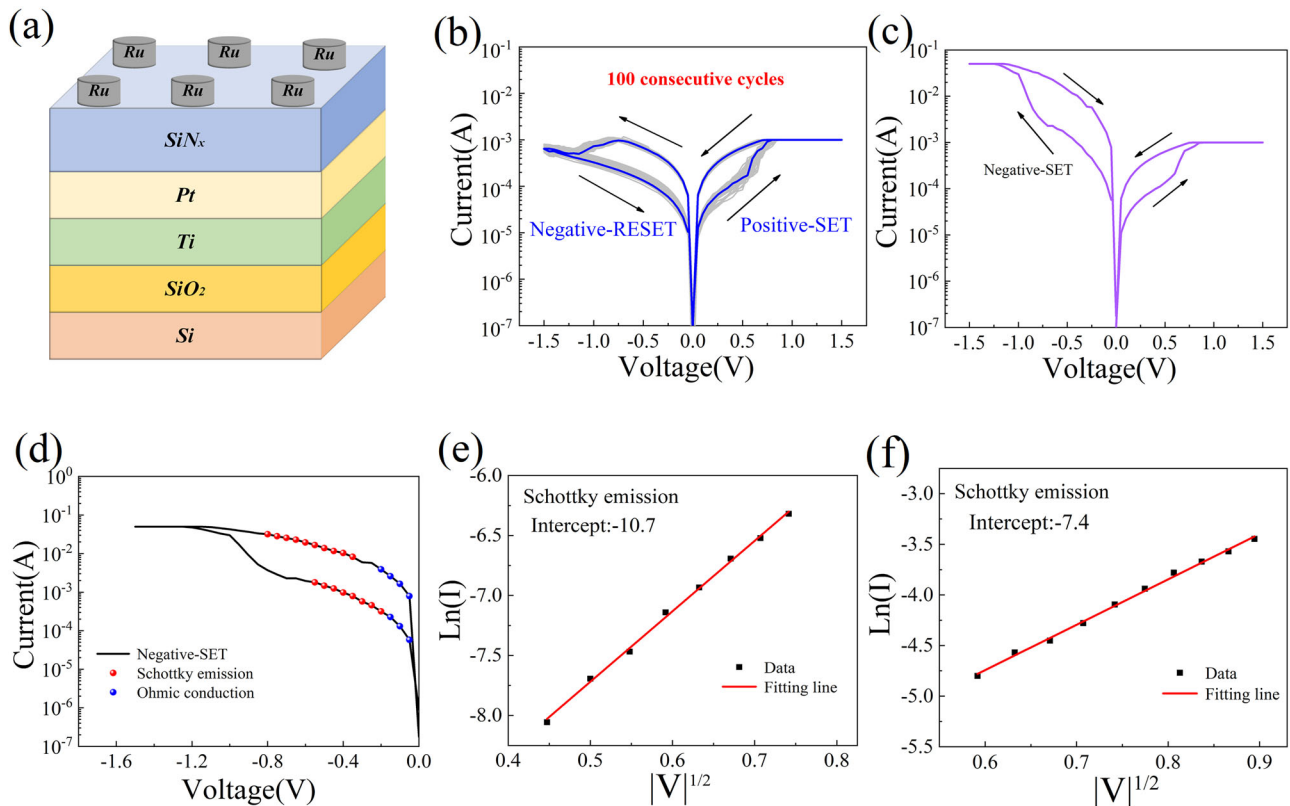


Fig. 1 | Electrical properties of Pt/SiN_x/Ru. a Schematic diagram of Pt/SiN_x/Ru Valence change memory. **b** The 100 I-V of Pt/SiN_x/Ru Valence change memory. **c** I-V characteristics for negative-SET. **d** Current conduction mechanism fitting

results of for negative-SET process. **e** Ln(I) vs $V^{1/2}$ re-plot between 0.2 V and 0.55 V for negative low resistance state. **f** Ln(I) vs $V^{1/2}$ re-plot between 0.35 V and 0.8 V for ultra-low resistance state.

regulate the HRS current level¹⁹. The above research results indicate that the passivation effect of hydrogen on defects could lead to a significant change in VCM current level, while abnormal increase of current level under negative bias is a typical feature of negative-SET. Therefore, it naturally raises the issue whether there is a correlation between the occurrence of negative-SET and the change in current levels caused by hydrogen passivation defects. At present, there are no reports on this issue and relevant research is urgently needed. A large number of studies on SiN_x-based VCM have been reported in previous researches, showing that SiN_x-based VCM have good data storage characteristics^{20–22}.

In this work, we use Pt and Ru inert electrodes with different hydrogen diffusion coefficients to construct SiN_x-based VCM, and the relationship between hydrogen ion movement and the occurrence of negative-SET is studied. A negative-SET process is observed in the Pt/SiN_x/Ru VCM. It is proposed that the diffusion of hydrogen ions from switching layer to the electrode is the key cause of the occurrence of the negative-SET process. Finally, a physical mechanism model of negative-SET in VCM is proposed.

Results and discussion

Electrical characteristics and fitting results

Figure 1b shows 100 consecutive I-V cycles of the VCM after applying the positive forming bias. During 100 cycles, the device exhibits stable bipolar RS behaviors, and the resistance value and operating voltage fluctuates slightly. However, after around 130 cycles, the device can not RESET under negative bias and the current continues to increase. A similar SET process occurred, that is, negative SET, as shown in Fig. 1c. For the analysis of the negative-SET phenomenon from the perspective of resistance changes is shown in Supplementary Fig. S4 in Supplemental Material. After negative-SET, the device can not return-back to HRS again, leading to irreversible RS behavior, which significantly affects reliability of the device. The device-to-device variability and cycle-to-cycle variability is shown in Supplementary Figs. S2 and S3 in Supplemental Material, respectively. For the retention characteristics of the device is shown in Supplementary Fig. S5 in Supplemental Material.

In order to clearly claim the reason for the occurrence of negative SET process, the current conduction mechanism of the negative SET process is

Fig. 2 | Linear fitting for the I-V curve. Fitting results for the Pt/SiN_x/Ru devices of a the 1st cycle, b the 100th cycles.

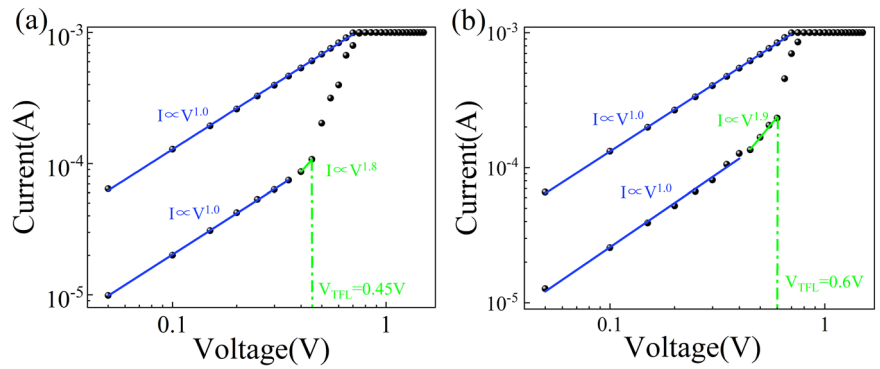


Table 2 | The R-square values of the fitting process in Fig. 1e, f

Resistive state	NLRS	ULRS
Voltage	-0.2 V → -0.55 V	-0.35 V → -0.8 V
R-squared values	0.99756	0.99679

carefully studied, as shown in Fig. 1d. Here, we refer to the resistance state before the negative SET as the negative LRS (NLRS), and the resistance state after the negative SET as the ultra-low resistance state (ULRS). For NLRS and ULRS, it is found that the Ohmic conduction can be fitted well in the lower voltage region²³, and Schottky emission can be fitted well in the higher voltage region²⁴. Figure 1e, f shows the linear fitting curves of Ln(I) and V^{1/2} of the NLRS and ULRS in the voltage range 0.2–0.55 V and 0.35–0.8 V respectively, indicating that the current conduction within this range is mainly based on Schottky emission²⁵. The Schottky emission model can be computed as²⁶:

$$J = A^* T^2 \exp\left[\frac{-q(\phi_B - \sqrt{qE/4\pi\epsilon_0\epsilon_r})}{kT}\right] \quad (1)$$

where A* is the Richardson constant, ϕ_B , J, E, q, ϵ_0 , and ϵ_r are the Schottky barrier height (SBH), the current density, the electric field, the electric charge, the permittivity of vacuum, and the relative permittivity, respectively.

According to Eq. (1), intercept of Ln(I) against V^{1/2} relation can be expressed as²⁷:

$$b = \ln(A^* ST^2) - \frac{q\phi_B}{kT} \quad (2)$$

According to Eq. (2), it can be concluded that the absolute value of the intercept is directly proportional to SBH²⁴. It is reported that a large number of defects would reduce the SBH of the contact interface²⁸. The absolute values of the Schottky intercepts of NLRS and ULRS are 10.7 and 7.4, respectively. From NLRS to ULRS, the absolute values of Schottky intercepts decrease, indicating that the SBH at the Ru/SiN_x interface decreases and the number of defects increases.

To further clarify the causes of negative-SET process in Pt/SiN_x/Ru VCM, the change of current conduction mechanism of Pt/SiN_x/Ru VCM with the increase of cycle number before the occurrence of negative-SET is studied. As shown in Fig. 2, the current conduction mechanism of the 1st and the 100th I-V cycles is analyzed. For the 1st and the 100th cycles, the LRS are fully fitted by Ohmic conduction over the full voltage range, indicating that the Ru and Pt electrodes are connected by a complete conductive channel in SiN_x layer²⁹. For the 1st and the 100th cycles of HRS, when voltage is of 0.05–0.35 V and 0.05–0.40 V respectively, the HRS's slope is ~1, corresponding to Ohmic conduction ($I \propto V$). As the voltage increases to 0.40–0.45 V and 0.45–0.60 V respectively, the HRS's slope is ~2,

corresponding to Child's square law ($I \propto V^2$). After that, the current increases significantly with voltage increases. The above analysis shows that the HRS conduction mechanism of the 1st and the 100th cycle is well fitted by space charge limited conduction (SCLC) model³⁰.

In SCLC, V_{TFL} is a key parameter. V_{TFL} is defined as the voltage required to fill the traps²⁷. While the bias voltage reaches V_{TFL} in the strong injection mode, the traps get gradually saturated, resulting in a strong increase of the number of free electrons, thus explaining the increase of the current³¹.

V_{TFL} can be computed as²⁷:

$$V_{TFL} = \frac{qN_t d^2}{2\epsilon} \quad (3)$$

where q, N_t, d, and ϵ is the electric charge, the defect density, the thickness of thin films, and the static dielectric constant.

According to formula (3), the defect density in the SiN_x film is proportional to the V_{TFL} value when other parameters are constant. For the 1st and the 100th I-V cycles, the V_{TFL} is 0.45 and 0.6 V respectively, indicating that the defect density in SiN_x film increased with the increase of cycle number. Noted that above mentioned defects density can be understood as the total number of defects, which contain newly formed in this cycle and accumulated number of defects formed in previous cycles.

At the same time, we extracted the R-squared values of the fitting process in Fig. 1e, f and Fig. 2, and summarized the results in Tables 2 and 3, respectively. It can be seen that the R-squared values of all fitting processes exceed 99%, further demonstrating the reliability of the fitting results.

Current sweep mode tests

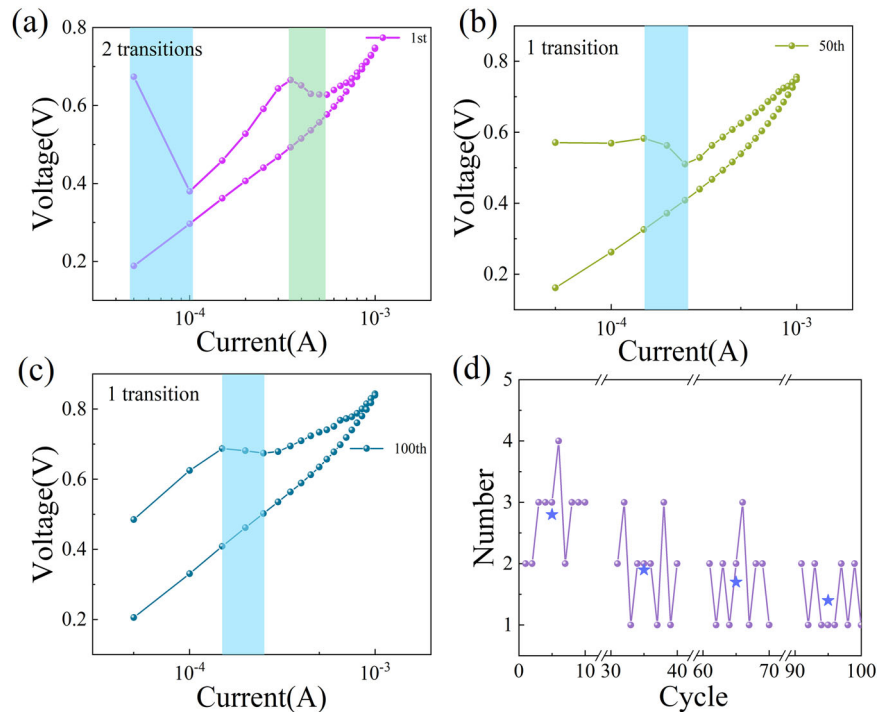
Compared with voltage sweep mode, current sweep mode can accurately capture the resistance reduction step during SET process, which is helpful to understand the cause of the negative-SET^{32,33}. Figure 3a–c shows the current sweep test results of the 1st, 50th and 100th cycles, respectively. As shown the blue shading in Fig. 3a, the first transition begins with a current of 5×10^{-5} A, and as the current increases the voltage suddenly drops and the resistance of device decreases. The second transition starts from the current of 3.5×10^{-4} A, and the voltage gradually decreases with current increases, and the resistance decreases, as shown the green shading in Fig. 3a. After two transition processes, the device remains LRS during backward sweeping, indicating a SET process is realized successfully by current sweep mode. With the cycle number increases, the device has only one transition process to complete the SET process and maintain a stable LRS in the 50th and 100th current sweep tests, as shown the shading in Fig. 3b, c.

In order to more clearly show the changing trend of transition number, the transition number in SET processes for the 1st–10th, 30th–40th, 60th–70th and 90th–100th cycles are counted, as shown in Fig. 3d. The purple ball represents the transition number for every SET processes, and the blue star represents the average transition number per ten SET processes. It can be obviously observed that as the cycle number increases, the average

Table 3 | The R-square value of the fitting process in Fig. 2

Cycle	The 1st I-V			The 100th I-V		
	LRS	HRS		LRS	HRS	
Voltage	0.05 V → 0.7 V	0.05 V → 0.35 V	0.4 V → 0.45 V	0.05 V → 0.7 V	0.05 V → 0.4 V	0.45 V → 0.6 V
R-squared values	0.99959	0.99980	1	0.99975	0.99435	0.99042

Fig. 3 | The current sweep mode test results of the Pt/SiN_x/Ru device. The current sweep mode test results of **a** the 1st, **b** the 50th, **c** the 100th. **d** Statistics on the transition number during 100 cycles. Error bars are generated from the standard deviation.



transition number gradually decreases. It is reported that under the action of electrical stress and thermal stress, the original bonding state changes in RS layer, leading to defects that constitute conductive filaments (CFs) formed during the set process, and formation process of these defects is related to the transition steps observed during the set process, that is, the more the number of defects formed in each set process, the greater the number of transitions^{34,35}. Thus, as the cycle number increases, the number of transition steps decreases, showing that as the cycle number increases, the number of newly formed defects in RS layer during each SET process (due to bonding state changed) decreases.

For SiN_x-based VCM, Si-dangling bonds (Si-DBs) are the major defects for the composition of CFs^{36,37}. In our previous research, we proposed that the origin of Si-DBs is caused by the initial formation during the SiN_x film deposition process and the broken of Si-N bond during the RS process (the broken of the Si-N bonds would lead to the formation of Si-DBs and the directional migration of nitrogen ions, resulting in a change in the resistance state of SiN_x-based VCM)^{38,39}. For Pt/SiN_x/Ru structure devices, Pt and Ru electrodes are inert electrodes, which only have the ability to electrical conductivity but do not have the nitrogen ions accommodation and adsorption ability. Therefore, the number of nitrogen ions in the SiN_x RS layer is constant, i.e., the migration of nitrogen ions can cause the movement of Si-DBs, but does not produce new Si-DBs defects. However, this is contrary to the above experimental analysis results, suggesting that there may be other ways for Si-DBs defects formation in addition to Si-N bonds broken.

Fourier transform infrared spectroscopy tests

The configuration of SiN_x thin film is examined using Fourier transform infrared (FTIR) spectroscopy, as shown in Fig. 4. The absorption bands at

763 cm⁻¹ and 2139 cm⁻¹ correspond to the Si-N stretching and Si-H stretching, respectively²⁰. It can be found that the peak of Si-N bonds is the strongest, indicating that the main component of the SiN_x film is composed of Si-N bonds. Moreover, Si-H bonds can also be clearly observed due to hydrogenation, indicating that hydrogen is present in SiN_x film. The preparation of SiN_x films using the PECVD process inevitably introduces hydrogen, which has been reported by many researchers⁴⁰⁻⁴². The bond energies of the Si-N and Si-H are 3.7 eV and 3.0 eV, respectively⁴³. Compared to bond energies of the Si-N, the smaller bond energies of Si-H makes it more easier to break and release hydrogen ions to participate in the RS process under the action of electric and thermal fields. That is to say, after the deposition process of SiN_x films is completed, the Si-DBs defects in SiN_x film might be formed by the following process: the Si-N bonds and Si-H bonds broken, leading to the movement of nitrogen and hydrogen ions, making the Si-DBs defects formed.

Construction of physical mechanism model

Based on the above analysis, a physical mechanism model of negative-SET in SiN_x-based VCM is proposed, as shown in Fig. 5. Jiang et al proposed that introduction of hydrogen in Al/a-SiN_x:H/p + -Si to control the Si-DBs CFs formation, which is conducive to obtaining ultra-low power SiN_x-based RRAM²⁰. Besides, due to the high diffusivity of hydrogen in metals, hydrogen in the environment can enter the RS layer through the electrode, causing significant changes in the RS characteristics of RRAM, which is why RRAM is recommended as hydrogen sensors⁴⁴. According to the above analysis and experimental results, we propose that in SiN_x-based VCM, nitrogen ions, as the main ions, dominate the RS process, while hydrogen ions, as the key ions, are responsible for the occurrence of negative-SET. During the forming process with positive bias, Si-DBs defects formed by the

broken of Si-N bonds and Si-H bonds, moving toward the Pt bottom electrode under the action of electric field, and a conical CF formed. At this time, the RS processes are controlled by the tip of CFs, and the Ru electrode is operation electrode, as shown in Fig. 5a.

Due to the inertivity of the electrode, the migration of nitrogen ions in SiN_x film can not produce new Si-DBs with the cycle number increases. Some hydrogen ions, which formed by Si-H bonds broken, could enter into the electrode under the action of electric field and continue to diffuse, resulting in a decrease in the hydrogen ions number in SiN_x film, as shown in Fig. 5b. Therefore, with the cycle number increases, Si-H bonds are replaced by Si-DBs defects in SiN_x films, resulting in an increase in the number of Si-DBs defects (corresponding to the analysis results of Fig. 2). Moreover, due to the partial hydrogen ions entering the electrode, the number of Si-H bonds within the SiN_x film decreases, making the number of transition steps related to Si-H bonds broken (bonding state changed) during SET process is reduced with cycles increase (corresponding to the analysis results of Fig. 3).

When negative-SET occurs, hydrogen ions at the Ru/SiN_x interface layer enter into the Ru electrode under the action of negative electric field, reaching a critical value, which significantly changes the properties of the Ru/SiN_x interface layer and reduces the SBH at the Ru/SiN_x interface layer, resulting in a sharp increase in current and the occurrence of negative-SET, as shown in Fig. 5c. In a word, RS behavior is caused by the movement of nitrogen and hydrogen ions in SiN_x-based RRAM devices, and the diffusion of hydrogen ions through the electrode is responsible for negative-SET.

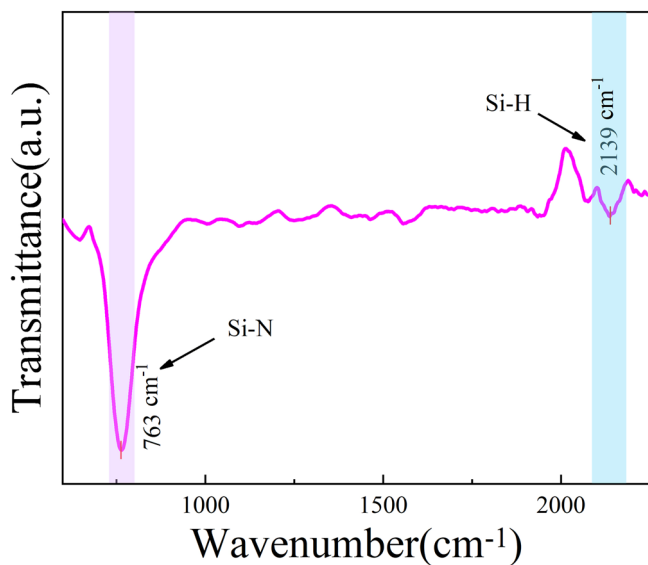


Fig. 4 | Fourier transform infrared spectroscopy of SiN_x films. The absorption bands at 763 cm⁻¹ and 2139 cm⁻¹ correspond to the Si-N stretching and Si-H stretching, respectively.

The Secondary Ion Mass Spectrometry (SIMS) results of the Pt/SiN_x/Ru device without voltage applied and after Negative-Set occurred is shown in Supplementary Fig. S6 in Supplemental Material.

The above model is verified by applying negative forming voltage to Pt/SiN_x/Ru device, as shown in Fig. 6. During the forming process with negative voltage applied, the device's current suddenly increases when the voltage is around -0.8 V, indicating that the forming process is completed; when a positive voltage is applied, the device current increases further as the voltage increases, as shown in Fig. 6a. This indicates that Pt/SiN_x/Ru device using negative forming voltage cannot complete the normal RS cycles, which has also been observed in our previous research on Pt/AlO_xN_y/Ta devices with negative forming process⁴⁵. It is reported that the CFs's shape and operation electrode can be controlled by changing forming voltage polarity⁴⁶. Thus, an inverted conical CFs formed during the negative forming process, and the operation electrode is Pt electrode, as shown in Fig. 6b. Compared with Ru, Pt has stronger inertness, making it easier to form thicker CFs in forming process, leading to the CFs is not easily broken, which might be the reason why normal RS cannot occur. Noted that Pt has a higher hydrogen diffusion coefficient than Ru^{47,48}. When the positive voltage is applied, hydrogen ions formed by the broken of the Si-H bonds are more easier to enter into the Pt electrode, making the number of Si-DBs defects in SiN_x film is further increased, resulting in stronger CFs formed and a higher current level. When positive voltages of 1.5 V, 1.8 V, 2.1 V, and 2.4 V are applied (after the negative forming is completed), the variation of the current level is shown in Fig. 6c, d. As applied voltage increases, the current level increases, which may be due to the fact that as the voltage increases, a larger electric field force causes more Si-H bonds broken, making more hydrogen ions enter into the Pt electrode and more Si-DBs formed inside SiN_x film, leading to the current level increases. The above experimental results verify the accuracy of proposed physical model.

The switching characteristics for SiN_x-based RRAM with different top electrode

To verify the above conclusions, keeping the Pt bottom electrode and the SiN_x resistive switching layer unchanged, we selected Ti as the top electrode to analyze the electrical characteristics of Pt/SiN_x/Ti device. Figure 7a, b shows the I-V characteristics and endurance characteristics of Pt/SiN_x/Ti device. We can see that Pt/SiN_x/Ti device can perform stable bipolar resistive switching and execute more than 300 I-V cycles; as the number of cycles increases, the LRS value gradually increases, and after 300 cycles, its LRS value is almost the same as the HRS value, indicating that the device no longer has resistive switching characteristics. In our previous research, it was pointed out that Ti, as an electrode with nitrogen adsorption ability, inevitably forms a TiN_x layer between SiN_x and Ti layer, which is the reason why the LRS value of the Pt/SiN_x/Ti device increases with the increase in cycles; the TiN_x layer spontaneously formed after completion of the device fabrication process, and its thickness and composition could change as the number of cycles increases⁴⁹. The hydrogen diffusion coefficient of TiN_x is much lower than Ru^{48,50}, which may be the reason why the Pt/SiN_x/Ti device did not occur negative-SET.

Fig. 5 | Models for the switching mechanism. a Formation of conductive filaments. b After some cycles, a small amount of hydrogen ions present in the Ru electrode. c After Negative-SET, a large number of hydrogen ions present in the Ru electrode.

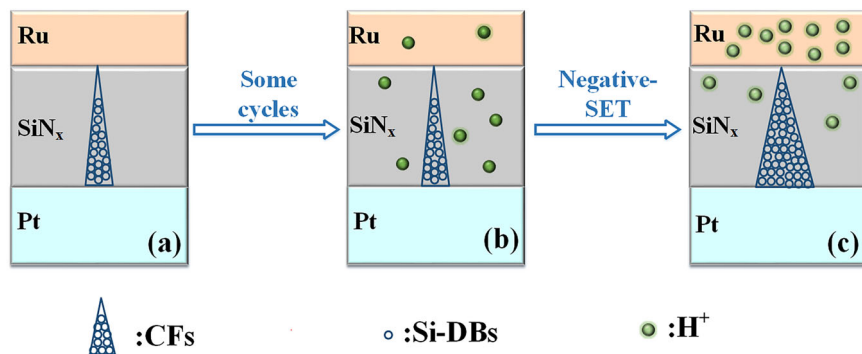


Fig. 6 | Electrical properties of Pt/SiN_x/Ru devices applying a negative forming voltage. **a** I-V characteristics of Pt/SiN_x/Ru Valence change memory with negative forming process. **b** Models for conductive filaments formed when negative forming voltage applied. **c** I-V curves with positive stop voltages of 1.5 V, 1.8 V, 2.1 V, and 2.4 V. **d** Enlarged view of ultra-low resistance state for (c).

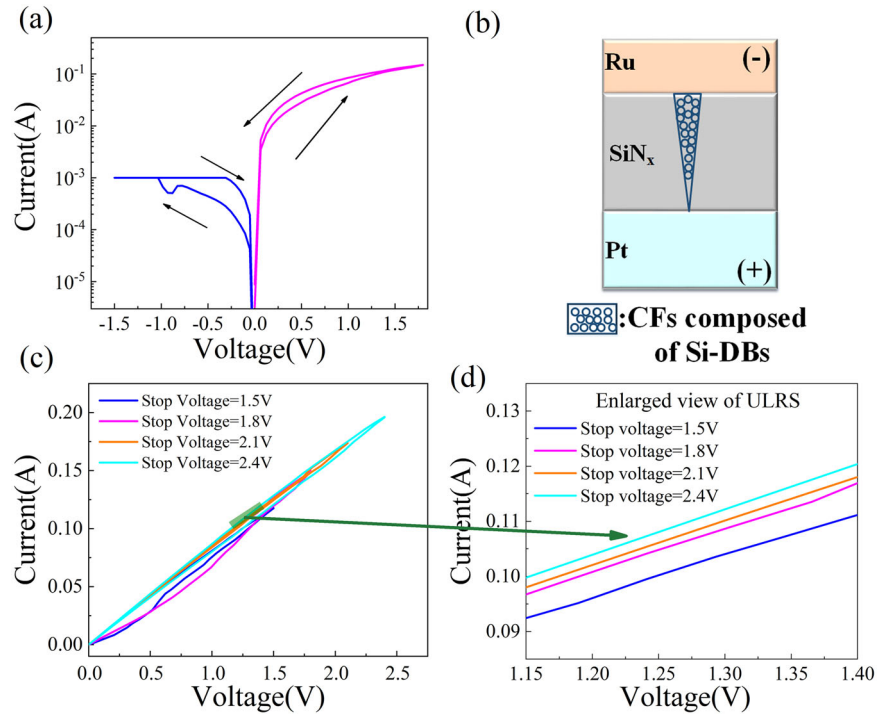
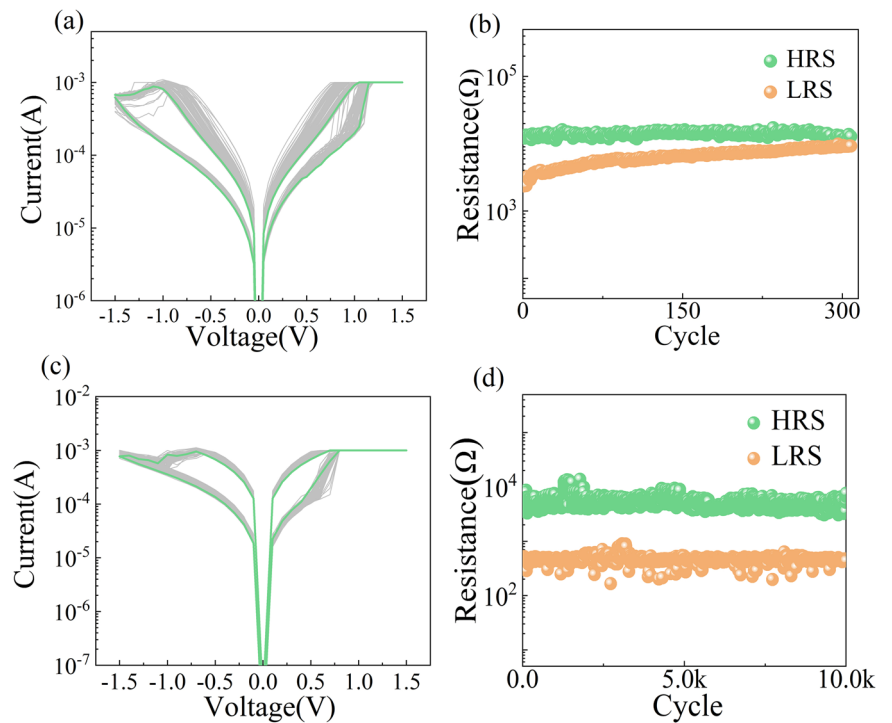


Fig. 7 | 100 consecutive cycles and endurance test results of Pt/SiN_x/Ti device and Pt/SiN_x/TiN_x/Ta device. **a** 100 consecutive cycles and **b** endurance test of Pt/SiN_x/Ti device. **c** 100 consecutive cycles and **d** endurance test of Pt/SiN_x/TiN_x/Ta device.



To further verify this experimental result, we used TiN_x as the insertion layer and prepared a Pt/SiN_x/TiN_x/Ta device. The I-V and endurance characteristics of the Pt/SiN_x/TiN_x/Ta device are shown in Fig.7c, d. This device did not occur negative-SET for more than 10,000 cycles and maintained stable switching, further proving that the low hydrogen diffusion coefficient of TiN_x may contribute to the improvement of the reliability of VCM devices.

Conclusions

In summary, the negative-SET process has been investigated in Pt/SiN_x/Ru devices. A negative-SET process is observed after some normal RS cycles in Pt/SiN_x/Ru devices with positive forming process. By current sweep tests and the analysis of current conduction mechanism, it is believed that the diffusion of hydrogen ions from RS layer to the electrode is the key reason for the occurrence of negative-SET. This study suggests that the role of

hydrogen ions in the RS process should be incorporated into the RRAM model, and we should pay more attention to the influence of hydrogen diffusion on the characteristics of VCM, especially on reliability, which provide ideas for improving the reliability by regulating the hydrogen diffusion coefficient of the electrode.

Methods

Device fabrication and characterization

The schematic diagrams of Pt/SiN_x/Ru VCM is shown in Fig. 1a. For the sample preparation, a 20-nm Ti adhesion layer and a 100-nm Pt bottom electrode (BE) were deposited on the SiO₂/Si (300 nm/500 μm) substrate by DC sputtering at room temperature. Then, 15-nm SiN_x films as switching layer were deposited through PECVD using SiH₄ and NH₃ as the reaction gases. Final, a 20-nm Ru top electrode (TE) was deposited on SiN_x films by DC sputtering at room temperature. The top-view image of the Scanning electron microscope (SEM) and the cross-sectional image of the Transmission electron microscope (TEM) of the Pt/SiN_x/Ru VCM is shown in Supplementary Fig. S1 in Supplemental Material.

Device electrical and materials tests

In the test of the Pt/SiN_x/Ru device, ground the Pt electrode and set the Ru electrode as the operation electrode. Electrical properties were measured using a Keysight B2901b. Fourier transform infrared spectroscopy was measured using BRUKER VERTEX 70v. The Scanning electron microscope was measured using Hitachi S-4800. The Transmission electron microscope was measured using Thermo Scientific Talos F200X. The Secondary Ion Mass Spectrometry was measured using IONTOF/M6.

Supplemental Material Scanning electron microscope (SEM) and Transmission electron microscope (TEM) plots of Pt/SiN_x/Ru, device-to-device and cycle-to-cycle test results of Pt/SiN_x/Ru, endurance and retention test results of Pt/SiN_x/Ru, resistance change of Negative-SET process, and Secondary Ion Mass Spectrometry (SIMS) results of the Pt/SiN_x/Ru device without voltage applied and after Negative-Set occurred are presented in the supplemental material.

Data availability

The data that support the findings of this study are available from the corresponding author upon reasonable request. Source data are provided with this paper (see Supplementary Data).

Received: 14 May 2025; Accepted: 21 October 2025;

Published online: 24 November 2025

References

- Kaniselvan, M., Jeon, Y. R., Mladenovic, M., Luisier, M. & Akinwande, D. Mechanisms of resistive switching in two-dimensional monolayer and multilayer materials. *Nat. Mater.* **24**, 1346–1358 (2025).
- Milozzi, A., Ricci, S. & Ielmini, D. Memristive tonotopic mapping with volatile resistive switching memory devices. *Nat. Commun.* **15**, 2812 (2024).
- Ielmini, D. & Pedretti, G. Resistive Switching Random-Access Memory (RRAM): applications and requirements for memory and computing. *Chem. Rev.* **125**, 5584–5625 (2025).
- Lastras-Montaño, M. A. & Cheng, K.-T. Resistive random-access memory based on ratioed memristors. *Nat. Electron.* **1**, 466–472 (2018).
- Jeon, K. et al. Self-rectifying resistive memory in passive crossbar arrays. *Nat. Commun.* **12**, 2968 (2021).
- Wang, S. et al. Random resistive memory-based deep extreme point learning machine for unified visual processing. *Nat. Commun.* **16**, 960 (2025).
- Goul, R. et al. Atomic-scale tuning of ultrathin memristors. *Commun. Phys.* **5**, 260 (2022).
- Strukov, D. B., Snider, G. S., Stewart, D. R. & Williams, R. S. The missing memristor found. *Nature* **453**, 80–83 (2008).
- Sun, Y., Wen, D. & Sun, F. Eliminating negative-set behavior by adding a graphene blocking layer in resistive switching memory devices based on epoxy resin. *Appl. Phys. Express* **12**, 074006 (2019).
- Niu, Y. et al. Improved Al₂O₃ RRAM performance based on SiO₂/MoS₂ quantum dots hybrid structure. *Appl. Phys. Lett.* **120**, 022106 (2022).
- Mahata, C. et al. SiO₂ layer effect on atomic layer deposition Al₂O₃-based resistive switching memory. *Appl. Phys. Lett.* **114**, 182102 (2019).
- Ismail, M., Hashmi, A., Rana, A. M. & Kim, S. Eradicating negative-set behavior of TiO₂-based devices by inserting an oxygen vacancy rich zirconium oxide layer for data storage applications. *Nanotechnology* **31**, 325201 (2020).
- Jia, Y. et al. A consistent model for gradual, abrupt, and abnormal reset phenomena in bipolar/unipolar metal oxide RRAMs. *IEEE Trans. Electron Devices* **71**, 3142–3149 (2024).
- Park, J. et al. Improved reset breakdown strength in a HfOx-based resistive memory by introducing RuOx oxygen diffusion barrier. *AIP Adv.* **6**, 055114 (2016).
- Wang, D. et al. Recovery of cycling-induced endurance failed HfOx based memristive devices by utilizing oxygen plasma treatment. *Appl. Phys. Lett.* **115**, 243105 (2019).
- Cox, H. R. J. et al. The role of hydrogen in ReRAM. *Adv. Mater.* **36**, 2408437 (2024).
- Duan, W. Observation of H-ion migration in a low-temperature-processed boehmite layer for nonvolatile memory. *ACS Appl. Electron. Mater.* **2**, 3711–3716 (2020).
- Lee, D., Chae, M., Song, H.-K. & Kim, H.-D. Ultra-low operation current and abnormal bipolar switching phenomena of hydrogen-passivated HfO₂ memristive devices for low power artificial neural network applications. *Ceram. Int.* **49**, 17497–17505 (2023).
- Wang, J.-C., Hsu, C.-H., Ye, Y.-R., Ai, C.-F. & Tsai, W.-F. Performance improvement of gadolinium oxide resistive random access memory treated by hydrogen plasma immersion ion implantation. *J. Vacuum Sci. Technol. A* **32**, 02B108 (2014).
- Jiang, X. et al. a-SiNx:H-based ultra-low power resistive random access memory with tunable Si dangling bond conduction paths. *Sci. Rep.* **5**, 15762 (2015).
- Gismatuln, A. A. et al. Charge transport mechanism in the metal-nitride-oxide-silicon forming-free memristor structure. *Appl. Phys. Lett.* **116**, 203502 (2020).
- Sun, B., Han, X., Xu, R. & Qian, K. Uncovering the indium filament formation and dissolution in transparent ITO/SiNx/ITO resistive random access memory. *ACS Appl. Electron. Mater.* **2**, 1603–1608 (2020).
- Lin, S.-K. et al. Improving performance by inserting an indium oxide layer as an oxygen ion storage layer in HfO₂-based resistive random access memory. *IEEE Trans. Electron Devices* **68**, 1037–1040 (2021).
- Xia, Q. et al. Impact of forming compliance current on storage window induced by a gadolinium electrode in oxide-based resistive random access memory. *IEEE Trans. Electron Devices* **65**, 96–100 (2018).
- Lin, C.-Y. et al. Effects of varied negative stop voltages on current self-compliance in indium tin oxide resistance random access memory. *IEEE Electron Device Lett.* **36**, 564–566 (2015).
- Zhou, K.-J. et al. Abnormal high resistive state current mechanism transformation in Ti/HfO₂/TiN resistive random access memory. *IEEE Electron Device Lett.* **41**, 224–227 (2020).
- Chiu, F.-C. A review on conduction mechanisms in dielectric films. *Adv. Mater. Sci. Eng.* **2014**, 1–18 (2014).
- Allena, M. W. & Durbin, S. M. Influence of oxygen vacancies on Schottky contacts to ZnO. *Appl. Phys. Lett.* **92**, 122110 (2008).
- Chen, P.-H. et al. Obtaining lower forming voltage and self-compliance current by using a nitride gas/indium-tin oxide insulator in resistive random access memory. *IEEE Trans. Electron Devices* **63**, 4769–4775 (2016).

30. Jiang, P. F. et al. Enhanced switching stability in forming-free SiNx resistive random access memory devices with low power consumptions based on local Pt doping in a stacked structure. *Adv. Electron. Mater.* **5**, 1800739 (2019).
31. Shen, X. et al. Effect of crystallinity on the performance of AlN-based resistive random access memory using rapid thermal annealing. *Appl. Phys. Lett.* **118**, 183503 (2021).
32. Chen, B. et al. A novel operation scheme for oxide-based resistive-switching memory devices to achieve controlled switching behaviors. *IEEE Electron Device Lett.* **32**, 282–284 (2011).
33. Khanna, S. P., Singh, S., Suman, C. K., Kumar, N. & Dabi, A. Multilevel non-volatile memristive response in e-textile. *IEEE Trans. Electron Devices* **70**, 468–472 (2023).
34. Zhou, F., Chang, Y.-F., Fowler, B., Byun, K. & Lee, J. C. Stabilization of multiple resistance levels by current-sweep in SiOx-based resistive switching memory. *Appl. Phys. Lett.* **106**, 063508 (2015).
35. Wu, X., Ge, R., Akinwande, D. & Lee, J. C. Understanding of multiple resistance states by current sweeping in MoS(2)-based non-volatile memory devices. *Nanotechnology* **31**, 465206 (2020).
36. Yang, M., Wang, H., Ma, X., Gao, H. & Wang, B. Effect of nitrogen-accommodation ability of electrodes in SiNx-based resistive switching devices. *Appl. Phys. Lett.* **111**, 233510 (2017).
37. Zhang, Z. F. et al. Effect of thickness of metal electrode on the performance of SiNx-based resistive switching devices. *Appl. Phys. Lett.* **114**, 042102 (2019).
38. Guo, J. et al. Influence of Nitrogen Adsorption of Doped Ta on Characteristics of SiNx-Based Resistive Random Access Memory. *Phys. Status Solidi a* **216**, 1900540 (2019).
39. Qiu, X. et al. Bipolar and complementary resistive switching induced by barrier regulation based on compliance current. *Appl. Phys. Lett.* **124**, 233509 (2024).
40. Karunakaran, B., Chung, S. J., Velumani, S. & Suh, E. K. Effect of rapid thermal annealing on the properties of PECVD SiNx thin films. *Mater. Chem. Phys.* **106**, 130–133 (2007).
41. Wan, G. J. et al. In vitro investigation of hemocompatibility of hydrophilic SiNx:H films fabricated by plasma-enhanced chemical vapor deposition. *Surf. Coat. Technol.* **200**, 1945–1949 (2005).
42. Alamgeer et al. Enhanced field-assisted passivation and optical properties improvement of PECVD deposited SiNx:H thin film. *Optical Mater.* **162**, 116885 (2025).
43. McPherson, J. W. & Mogul, H. C. Underlying physics of the thermochemical E model in describing low-field time-dependent dielectric breakdown in SiO₂ thin films. *J. Appl. Phys.* **84**, 1513–1523 (1998).
44. Haidry, A. A., Ebach-Stahl, A. & Saruhan, B. Effect of Pt/TiO₂ interface on room temperature hydrogen sensing performance of memristor type Pt/TiO₂/Pt structure. *Sens. Actuators B Chem.* **253**, 1043–1054 (2017).
45. Duan, Y. et al. Dynamic evolution process from bipolar to complementary resistive switching in non-inert electrode RRAM. *Appl. Phys. Lett.* **120**, 203506 (2022).
46. Chen, P.-H. et al. Bulk oxygen-ion storage in indium–tin–oxide electrode for improved performance of HfO₂-based resistive random access memory. *IEEE Electron Device Lett.* **37**, 280–283 (2016).
47. Čermák, J., Kufudakis, A. & Gardavská, G. Diffusivity of hydrogen in platinum and the diffusionelastic phenomenon. *J. Less Common Met.* **63**, 1–P8 (1979). P.
48. Soroka, O. et al. Hydrogen diffusion through Ru thin films. *Int. J. Hydrog. Energy* **45**, 15003–15010 (2020).
49. Duan, Y., Gao, H. & Yang, Y. Analyzing switching variability of SiNx-based RRAM in terms of Joule heating dissipation. *Appl. Phys. Lett.* **125**, 173501 (2024).
50. Triestram, L. & Polfus, J. M. Hydride ion diffusion along grain boundaries in titanium nitride. *Acta Mater.* **270**, 119853 (2024).

Acknowledgements

This work was supported by the Shaanxi Association for Science and Technology Youth Talent Support Program (Program No.20240147), Scientific Research Program Funded by Education Department of Shaanxi Provincial Government (Program No.24JK0292), Research business expenses of Baoji University of Arts and Sciences, the National Natural Science Foundation of China, under contact Nos. 11304237 and 11704297, Union Foundation of Ministry of Education of China (Fabrication and mechanism of nitride resistive switch memory device), and by the Natural Science Foundation of Shaanxi Province, China (2018JQ6040).

Author contributions

Yiwei Duan conceived the idea. Xudong Feng and Yuqi Liu performed electrical characterization and materials characterizations. Haifeng Yang, Fei Liu, Yu Qian, and Yintang Yang guided the research. All authors contributed to interpreting the data and writing the manuscript, and all authors have given approval to the final version of the manuscript.

Competing interests

The authors declare no competing interests

Additional information

Supplementary information The online version contains supplementary material available at <https://doi.org/10.1038/s42005-025-02386-6>.

Correspondence and requests for materials should be addressed to Fei Liu, Yu Qian or Yintang Yang.

Peer review information *Communications Physics* thanks Horatio Cox and Yao-Feng Chang for their contribution to the peer review of this work.

Reprints and permissions information is available at <http://www.nature.com/reprints>

Publisher's note Springer Nature remains neutral with regard to jurisdictional claims in published maps and institutional affiliations.

Open Access This article is licensed under a Creative Commons Attribution-NonCommercial-NoDerivatives 4.0 International License, which permits any non-commercial use, sharing, distribution and reproduction in any medium or format, as long as you give appropriate credit to the original author(s) and the source, provide a link to the Creative Commons licence, and indicate if you modified the licensed material. You do not have permission under this licence to share adapted material derived from this article or parts of it. The images or other third party material in this article are included in the article's Creative Commons licence, unless indicated otherwise in a credit line to the material. If material is not included in the article's Creative Commons licence and your intended use is not permitted by statutory regulation or exceeds the permitted use, you will need to obtain permission directly from the copyright holder. To view a copy of this licence, visit <http://creativecommons.org/licenses/by-nc-nd/4.0/>.

© The Author(s) 2025